Model investigation of aerofoil sails as auxiliary ship propulsion devices

M.K. Lambrecht,[1] J.W. Klintworth,[1] M.G. Jordaan[2] and E.A. Bunt[1]

(Received December 1993; Final version September 1994)

Abstract

In recent years, one aspect of the resurgence of interest in saving fossil fuel has been a proposal to use aerofoil sails as an auxiliary form of ship propulsion. To examine the possible effect on running costs of the use of such sails, a simplified model investigation, based on the configuration employed by a Japanese cargo vessel, the 'Shin Aitoku Maru', was undertaken, using models of a RINA Standard Tanker YB fitted with two vertically pivotted NACA $63_3 - 018$ aerofoil section sails on the foredeck. The tests involved basically (a) hydrodynamic testing of a 1:100 scale model ship hull in a towing basin; (b) aerodynamic testing (with and without sails) of a 1:300 above-waterline ship model in a low speed wind tunnel; followed by (c) supplementary towing basin testing of a 1:300 ship model (using the same sails), with a fan mounted on the towing carriage to simulate the effects of wind veering from $0°-180°$ to the forward direction of travel. The combined results were scaled up for 'standard' (prototype) conditions of a required ship-speed of 11.7 knots, operating in a true wind speed of 13.25 knots (using wind data for a well-used shipping route) to give a polar diagram of expected fuel savings as a function of incidence and angle to the true wind (between $0°$ and $180°$). A maximum saving of about 10% for a true wind direction of $90°$ was predicted – which is well below the claim for the Japanese vessel that the sails can provide up to 50% of the power required to travel at 12 knots.

Nomenclature

A	Area, m^2
AR	Aspect ratio
ARC	Ahead resistance coefficient
A_T	Transverse projected area, m^2
C_D	Drag coefficient $\left(\frac{F_D}{\frac{1}{2}\rho A V_{aw}{}^2}\right)$
C_d	Drag coefficient of 2-dimensional wing
C_F	Force coefficient $\left(\frac{\text{Force}}{\frac{1}{2}\rho A V_{aw}{}^2}\right)$
C_f	Skin friction coefficient
C_L	Lift coefficient $\left(\frac{F_L}{\frac{1}{2}\rho A V_{aw}{}^2}\right)$
C_R	Resistance coefficient
C_T	Total resistance coefficient
FF	Drag, N
Fr	Froude number
F_A	Aerodynamic force, N
F_D	Drag force, N
F_H	Hydrodynamic force, N
F_L	Lift force, N
F_p	Propulsion force, N
Re	Reynolds number
R_R	Residual resistance, N
R_t	Total ship resistance, N
r	Moment arm, m
S	Ship wetted area, m^2
SF	Side force, N
SI	Ship side force, N
V_{aw}	Apparent wind speed, m/s
V_R	Relative wind speed, m/s
V_S	Ship speed, m/s
V_w	True wind speed, m/s
WF	Forward force, N
α	Apparent wind direction (relative to heading), (deg)
β	True wind direction (relative to heading), (deg)
γ	Leeway angle, (deg)
δ	Incidence angle, (deg)
δ_o	Incidence angle of 2-dimensional wing, (deg)
ν	Kinematic viscosity, m^2/s
ρ	Density, kg/m^3

Introduction

Steam turbines, compression ignition engines and (latterly) gas turbines almost universally replaced sail as a means of propulsion to avoid the disadvantages of complete dependence on the weather as soon as reliable and efficient designs of propulsion machinery became available. However, even in the early 19th century, steam was conceived merely as an adjunct to sail. Brunel's three great steamships (1838–1857) made provision for sail.

In recent years, however, the rapidly increasing cost of liquid fuel has stimulated renewed interest in various novel hull forms, as well as in the use of aerofoil sails whose aerodynamic behaviour in respect of lift and drag is superior to that of 'blown' sails, for purposes of assisted propulsion, and the addition of aerofoil sails to catamarans has recently been proposed.[1] The configuration of a modern Japanese cargo vessel, the 'Shin Aitoku Maru' [2] (which makes use of vertically pivotted aerofoils to facilitate continuous variation of their setting at the optimum angle of incidence in relation to wind direction and ship heading),

[1]School of Mechanical Engineering, University of the Witwatersrand, P.O. Wits, 2050 Republic of South Africa

[2]Energy Laboratory, Rand Afrikaans University, Johannesburg

suggested that a model investigation to estimate possible fuel savings would be of interest. A ship of this nature has a reasonably flush foredeck without cranes (which is therefore suitable for the mounting of aerofoils), together with a superstructure situated well aft to reduce disturbance of the air flow over the sails.

To establish data for optimum aerofoil settings as a function of varying wind strength and direction, both aerodynamic and hydrodynamic laboratory tests of a tanker model fitted with two vertically pivotted symmetrical aerofoil sails were conducted. This model, that of a RINA Standard Tanker, Model YB, was chosen since it was both available and of a suitable configuration for the mounting of sails. Details of the full scale tanker are given in Table 1.[3]

Table 1 Details of RINA Standard Tanker, Model YB [3]

Length on water line	122 m
Breadth	16.8 m
Draught	4.8 m
Block coefficient[3]	0.8
Displacement	7 340 t
Wetted surface	2 543 m^2

Full scale Tanker (see Appendix 3) resistance versus speed curves indicated that the drag increased rapidly above 12 knots ($Fr = 0.178$) so a speed of 11.7 knots was chosen as a representative ship speed.

The tests conducted involved

1. Hydrodynamic drag tests of a 1:100 scale model ship hull in a 15 m long towing basin at speeds ranging between 0.4 and 1 m/s; and
2. Aerodynamic testing (both with and without aerofoils) of a 1:300 scale model of an above-waterline ship model in a low speed wind tunnel capable of air speeds up to approximately 80 m/s.

These tests were supplemented by tests of a 1:300 'sail' model (using the same sails) operating in a simulated wind provided by a fan attached to the towing carriage – the 'wind' direction being variable in azimuth in relation to the model (between 0° and 180°).

Theory

Figure 1 shows the well-known lift force F_L and drag force F_D acting on an aerofoil operating at an angle of incidence δ between the chord line and the direction of the oncoming wind. The resultant of these two forces (acting through the aerodynamic centre) is the 'aerodynamic force' F_A.F_L and F_D are, respectively, given by

$$F_L = \frac{1}{2}\rho {V_{aw}}^2 A C_L \qquad (1)$$

[3]Block coefficient = $\frac{\text{immersed volume of hull}}{\text{volume of circumscribing 'block'}}$

and

$$F_D = \frac{1}{2}\rho {V_{aw}}^2 A C_D \qquad (2)$$

In the case of a finite wing, end effects modify two-dimensional results and are described in terms of the aspect ratio AR:

$$\delta = \delta_o + \frac{C_L}{\pi AR} \qquad (3)$$

where δ_o is the incidence of the 2-dimensional wing, and

$$C_D = C_d + \frac{{C_L}^2}{\pi AR} \qquad (4)$$

where C_d is the drag coefficient of the 2-dimensional wing.

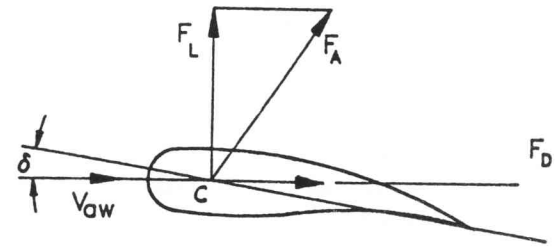

Figure 1 Force vector diagram for aerofoil

Figure 2(a) shows the relationship between the true wind vector V_w and the apparent wind vector V_{aw} for a ship moving at speed V_S. In Figure 2(b), which shows the forces to which the ship and aerofoil combination is subjected, the 'leeway angle' γ is the angle between the direction of motion and the ship's longitudinal centreline, and is normally only 2–3°; while δ is the angle of incidence between the chord of the aerofoil and the apparent wind vector V_{aw}. The propulsive force F_p (thrust) due to the action of the propeller is added vectorially to the aerodynamic force F_A, giving a resultant force equal and opposite to the hydrodynamic force F_H (total resistance).

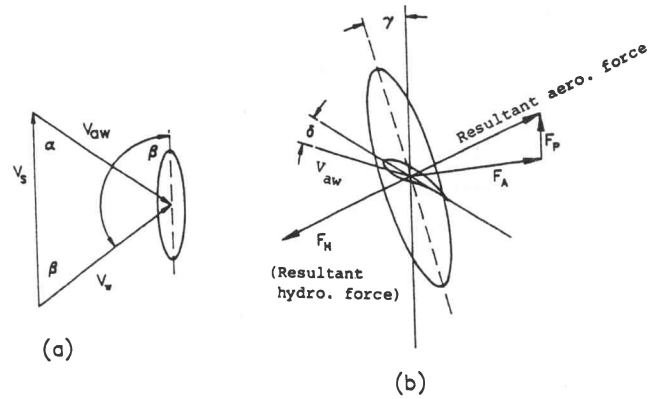

Figure 2 Wind vector diagram for ship

The hydrodynamic resistance of a ship is composed of 'residual' drag (mainly wave) and frictional drag (here assumed to be independent of each other). Frictional force may be calculated from the friction coefficient C_f given

(for turbulent flow) by the ITTC model-ship correlation line [4]

$$C_f = \frac{0.075}{(\log Re - 2)^2} \tag{5}$$

or for laminar conditions by Prandtl's equation [5]

$$C_f = \frac{0.455}{(\log Re)^{2.58}} \tag{6}$$

The latter expression was used here – there being very little difference between the formulae for the range of Re in the hydrodynamic experiments conducted. However $Re_{\text{transition}}$ (based on ship length) is considered to be given by

$$2 \times 10^5 \preceq Re_{\text{transition}} \preceq 4 \times 10^6 \tag{7}$$

within which range the model Re may be expected to fall.

The calculated friction force is subtracted from the model's total resistance to give the residual resistance. The latter is scaled according to the ratio of the displacements, and the ship's calculated friction force is then added to yield a predicted total resistance for the prototype vessel.

The superstructure resistance is expressed in terms of an ahead resistance coefficient (ARC) given by

$$ARC = \frac{\text{fore-and-aft component of wind resistance}}{\frac{1}{2}\rho V_R^2 A_T} \tag{8}$$

where A_T is the transverse projected area; V_R is the relative wind velocity.

It was found that ARS was approximately constant at a value of 8.8 for wind directions between 0° and 50° off the bow, showing that the diminished forward component of velocity was compensated by increasing projected area as the angle of attack increased.

Dynamic similarity

Aerodynamic testing (for scale factor of 1:300)

Full aerodynamic similarity demands that the Reynolds number (based, in the case of an aerofoil, on the chord) be preserved in model testing. This is normally impossible in tunnels operating at near atmospheric pressure – hence the popularity of pressurised tunnels to increase air density, and the use of high speed water tunnels (for 'aerodynamic' testing) to offset the Re inequality, since ν_{water} (say, 1.145×10^{-6} m/s) $\ll \nu_{\text{air}}$ (say, 1.51×10^{-5} m/s).

The representative prototype speed (= relative wind speed in still air) was chosen to be 11.7 knots (= 6.02 m/s). Even if a gale should raise the relative wind velocity to, say, 45 knots (= 23.17 m/s), the value of Re (using an assumed aerofoil chord of 15 m) would still be only

$$Re_{\text{chord}}\ (\text{prototype, sail}) = \frac{15 \times 23.17 \times 10^5}{1.51} = 23.03 \times 10^6$$

whereas at maximum tunnel speed (80 m/s), using a model chord of $\frac{15}{300} = 0.05$ m,

$$Re_{\text{chord}}\ (\text{model, sail}) = \frac{0.05 \times 80 \times 10^5}{1.51} = 2.64 \times 10^5$$

which is lower than such a prototype requirement by a factor of 87. [In practice, 2 velocities lower than 80 m/s were used (31.93 and 41.22 m/s), corresponding to convenient tunnel dynamic pressures of 0.6 and 1.0 kPa.] The wind tunnel speeds were thus far too low for correct dynamic similarity – but to have operated at much higher speed values would have raised the Mach number (which at 80 m/s was 0.23) to an unacceptably high value.

Hydrodynamic testing (for a scale factor of 1:100)

Dynamic similarity is here easier to achieve since the basis for model testing is the Froude number based on the ship's waterline length. For two similar ships running at equal Fr numbers, the total residual (wave-making)resistance is proportional to the displacement (or length factor cubed). The resistance coefficient is given by

$$C_R = \frac{R_R}{\frac{1}{2}\rho S V^2} \tag{9}$$

where S is the wetted area of the ship. For a representative prototype speed of, say, 12 knots (6.18 m/s),

$$Fr_{\text{length}}\ (\text{prototype, hull}) = \frac{6.18}{\sqrt{9.785 \times 122}} = 0.179\ ^4$$

which equates to the dynamically similar value (for the generation of identical surface wave patterns) of

$$Fr_{\text{length}}\ (\text{model, hull}) = \frac{0.62}{\sqrt{9.785 \times 1.22}}$$

for the model hull, i.e. the required speed is 0.62 m/s – which was within the towing tank operating range of 0.4 to 1 m/s.

Combined tests (using fan, ship scale factor of 1:300)

If Reynolds scaling be used for the aerodynamic effects, then at 6.5 m/s fan (centreline) air velocity (= 12.72 knots),

$$Re_{\text{chord}}\ (\text{model, sail}) = \frac{0.05 \times 6.5 \times 10^5}{1.51} = 21\,500$$

Again, this is lower by a further factor of 12 than the maximum tunnel Re for dynamic similarity. However, since it would have been out of the question to direct an air jet of much higher velocity at such a towed model for the sake of achieving Reynolds similarity, the results obtained using this arrangement can only be regarded as qualitative. (In consequence, little purpose would have been served by having a variable speed fan motor drive.)

[4] g is here taken as the actual Johannesburg (surface) value of 9.785 m/s ^{2}

Experimental

Model design

The reasons for the choice of a RINA Standard Tanker, Model YB, have been referred to above. The details of the 1:100 scale model are listed in Table 2, and further details are given in Appendix 2.

Table 2 Details of 1:100 scale model of RINA Standard Tanker, Model YB

Length on water line	1.22 m
Breadth	0.168 m
Draught	0.048 m
Block coefficient	0.8
Displacement	7.34 kg
Wetted surface	0.2543 m^2

Corresponding dimensions applied to the 1:300 scale model used. The selection of a suitable sail section (NACA 63_3–018 [3]) rested on the following criteria:

1. This section is symmetrical, thereby making it possible for the ship to be able to sail equally on port or starboard tack without the necessity of reversing the sail shape to suit the altered wind angle.
2. The drag coefficient versus lift coefficient curve (see Figure A-1 in Appendix 1) is very flat compared with sections of varying thickness ratio and varying maximum thickness positions, i.e. the drag coefficient remains low over a large range of angles of attack, thereby lending leniency to the setting of the sail.
3. The moment coefficient remains approximately zero for the full range of lift coefficient, thus reducing the force required to change the angle of the sail during operation – assuming that the sail is pivotted at the aerodynamic centre of the section.
4. The stall point is not completely sudden, again allowing a margin of error in the setting of the dial. (This is also important if the wind should suddenly change direction by a few degrees.)

The required sail area was based on a consideration of the average wind velocities which the prototype ship would be expected to encounter. To gauge these, a high density traffic shipping route within the North Atlantic anti-cyclone (New York to Scilly Isles) was selected, and a routing chart showing wind rosettes along this route was examined. The route was divided into 3 sectors, and the frequency and direction of a particular speed range were read off from individual rosettes. Average wind speeds and directions were then calculated from:

Average wind speed

$$= \sum (\text{frequency}) \,.\, (\text{mean speed of range}) \qquad (10)$$

Average wind direction

$$= \frac{\sum (\text{frequency}) \,.\, (\text{mean speed of range}) \,.\, (\text{true incidence})}{\text{average wind speed}} \qquad (11)$$

These three sectors yielded the results in Table 3.

Table 3 Analysis of wind data

Sector	Average speed, knot	Average wind direction, degree
Western	11.56	120
Central	13.86	123
Eastern	14.28	109

The overall average result was therefore a wind speed of 13.23 knots from a direction 117° off the bow. Details are given in Appendix 1 of the calculation of a prototype wing area of 878 m^2 using tanker thrust data (Appendix 3 [3]) to contribute, say, 20% of the propulsive thrust required on the route selected. The chord length of the aerofoil was limited by the width of the ship – as too much overhang could have led to possible damage to harbour facilities. Assuming that the aerofoil is pivotted at the aerodynamic centre, i.e. at a point 28% along the chord from the leading edge, use of a chord value of, say, 15 m would give a (maximum) overhang of the trailing edge of the sail over the side of 2.4 m when the sail is at 90° to the longitudinal centre line – which would seem to be acceptable. However, to achieve the required area in a single sail of this chord value would require a span of 58.5 m, which would result in a dangerously high centre of effort and hence large resultant moment at the base of the sail. To alleviate this, 2 sails, each having half the above span (actually, 30 m) were selected for modelling. (Although the resulting aspect ratio of 2 is low from the point of view of efficiency, this value appears to be similar to that of the sails installed on the 'Shin Aitoku Maru' [2].)

The positioning of the pivots of the sails (as seen in the side elevation of the model, Figure 3) was such as to attempt to bring the centre of effort of the combination of sails and superstructure to the centre of the ship. (However, any deviation of this position from the ship's centre could be measured as a yawing moment during wind tunnel testing.)

The 1:300 scale aerofoils were machined in aluminium on a milling machine to the co-ordinates specified in Appendix 1, and were attached to aluminium pivots 5 mm in diameter.

Aerodynamic testing

For aerodynamic test purposes, a small closed circuit low speed wind tunnel was used, having a maximum wind velocity of 80 m/s; this had an elliptical cross-section, with a major (horizontal) diameter of 919 mm, and a minor (vertical) diameter of 615 mm. The fan was driven by a variable speed D.C. motor and dynamic pressure was read by a pitot tube coupled to an inclined manometer with a

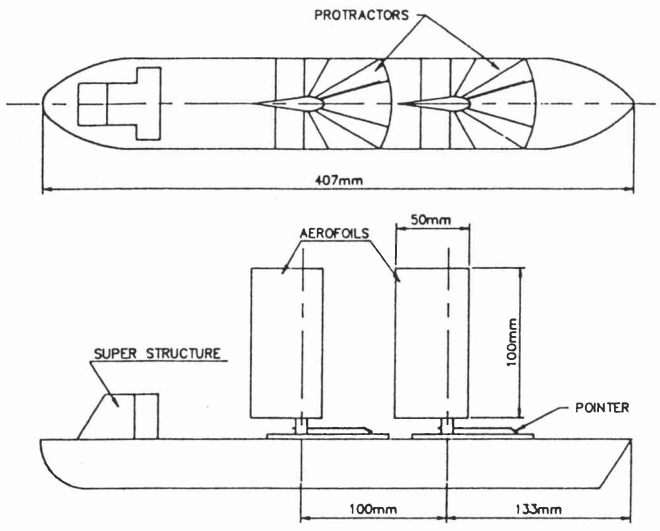

Figure 3 Model details

range of 2.5 kPa and resolution of 0.01 kPa. Boundary layer thickness in the working section was approximately 100 mm. The ship model was mounted on a 500 mm square test table to simulate the sea surface; this was provided with an angle rose protractor (Figure 4) marked in 15° intervals to facilitate sail incidence setting. This table was attached to a 6-component Aerolab pyramidal balance by means of a 19-mm diameter steel rod. The balance was used to measure only drag, side force and yawing moment, the maximum balance readings being: Force, 228 N; Moment, 11.8 Nm. Balance output was transferred to an HP 3421 A data acquisition/control unit whereby 5 readings of each of the 3 channels used were averaged, the resolution being 10^{-4} mV. All results were then processed on a Commodore 3032 computer.

Calibration of the balance was performed by placing a standard T-beam in the pyramidal balance. This was then loaded in various directions with known weights in order to calibrate for side force, drag and yawing moments, and satisfactory linearity was obtained. During calibration for side force, the mounting support was loaded at different heights to determine the effect, if any, of differing moment arms. Negligible discrepancies in output were found. To determine the drag of the table alone (for purposes of subtracting this from the drag of table and ship when mounted together), the model table without ship was placed in the wind tunnel and the above 3 measurements repeated at a range of dynamic pressures up to 1.2 kPa. The result of this test highlighted an unexpected difficulty (Figure 5). Theoretically, this graph should be linear, since dynamic pressure $= \frac{1}{2}\rho V^2$ and drag is also $\propto$ (velocity)^2. The slightly concave-up shape of the curve was ascribed to the fact that as speed increased, the increased drag force caused an upward tilting of the table as a direct result of flexibility in the pyramidal balance; in fact, the table was seen to tilt up by as much as 3° at 1 kPa dynamic pressure, significantly increasing the projected area and hence the drag. To allow for this at, say, 0.6 kPa, a drag reading of 0.3412 mV, as given by Figure 5, was used for subsequent null reading conversions.

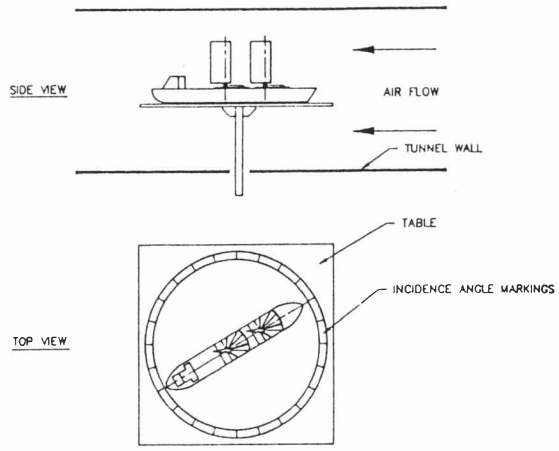

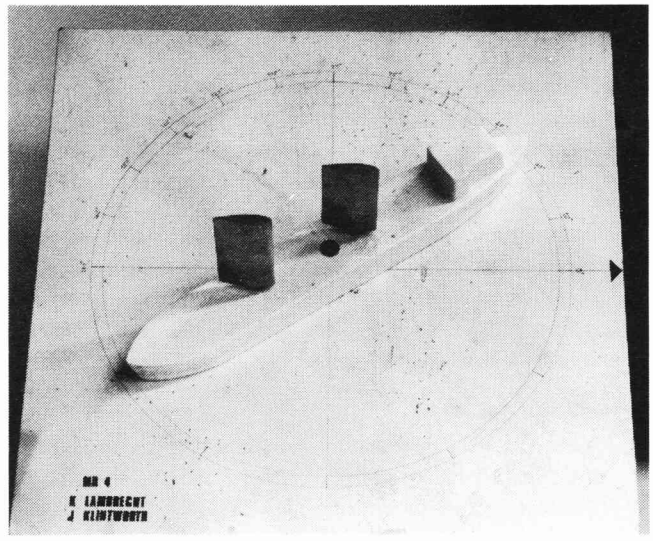

Figure 4 Aerodynamic model on testing table

The angles of the sails could be adjusted during tunnel running by inserting a wooden fork through the tunnel roof hatch (and thereby twisting the sails). Positioning of the ship model could likewise be adjusted during running by loosening the model attachment screw by the use of an extended screw driver which could also be passed through the tunnel roof hatch.

Further reference values were taken by testing the ship without sails in the wind tunnel. For dynamic pressures of 0.6 and 1.0 kPa, readings were made of side and forward force for the ship at incidence values ranging from 0° to 180°. In force coefficient form,

$$C_F = \frac{\text{Force}}{\frac{1}{2}\rho V^2 A} = \frac{\text{Force}}{(\text{Dyn. pres.})\,A}$$

To normalise the 2 curves at different dynamic pressures, a common (arbitrary) area is required. Figure 6 has therefore been plotted in terms of AC_F for the 2 values of dynamic pressure; the close correspondence of the 2

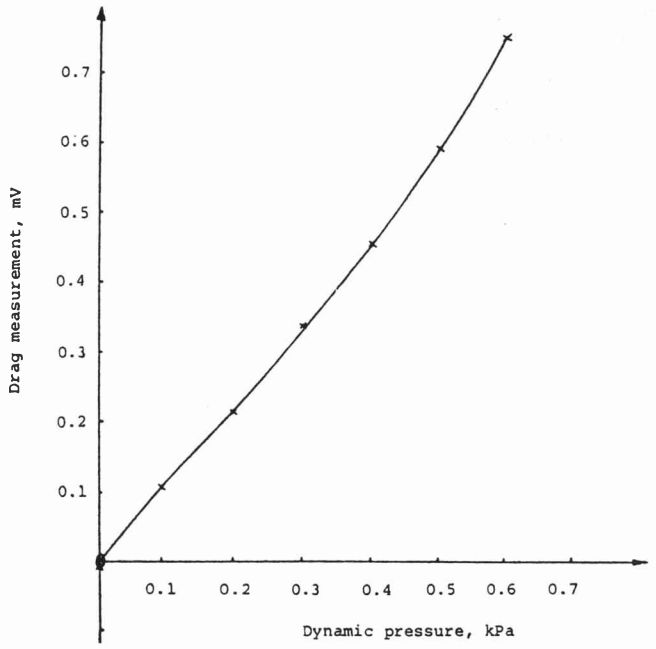

Figure 5 Drag measurement vs dynamic pressure for table alone

curves suggests good tunnel behaviour in respect of dynamical similarity – and hence acceptability of other results obtained in this way. Certain (repeatable) anomalies in these curves are discussed later.

Since balance drag and side forces apply in the direction of, and perpendicular to, the airflow, forward and side forces relative to the ship could be calculated by simple geometry:

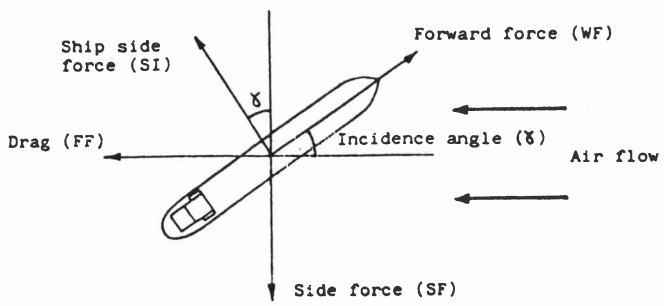

From this figure,

$$\begin{aligned} \text{Forward force } WF &= -FF\cos\gamma - SF\sin\gamma \\ \text{Side force } SI &= FF\sin\gamma - SF\cos\gamma \end{aligned}$$

Graphs of forward force (thrust) and ship side force could now be plotted for each incidence angle (Figure 7) to determine the best (maximum) driving force that could be expected under those conditions of wind strength and wind direction. [In Figure 7, the degree value entered on each plot (30°, 60°, etc.) represents the ship incidence angle in relation to the tunnel wind. For these tests, 'sail angle' represents the angle the chord of the aerofoil makes with the longitudinal axis of the ship, as shown in the following illustration for the case of a ship at an incidence angle of 35°. Both sails were normally set at the same angle.]

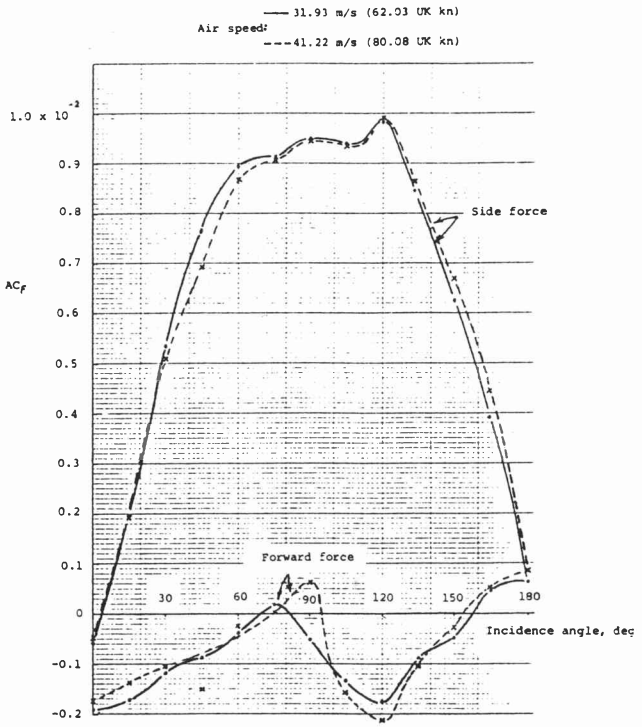

Figure 6 Aerodynamic tests – force coefficient vs incidence angle for hull without sails

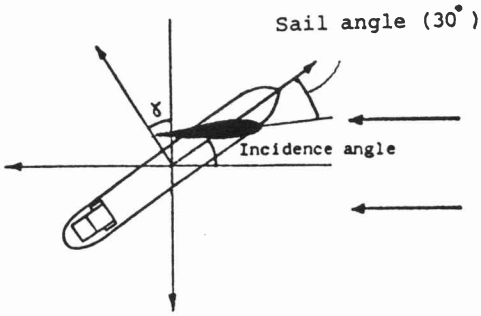

For each incidence angle setting, the sails were first 'feathered' (i.e. aligned at a sail angle of 0° in relation to the ship's heading); the sail angles were then increased in steps of 5° up to 25° (which is beyond the expected stall angle) and then in steps of 10° – with the aerofoil facing more and more into the tunnel wind. From these results, maximum force values (at any sail angle) were read off and Figure 8 drawn on a base of apparent incidence angle.

Since in such tunnel tests every effort is made to achieve uniform air flow over a test model (outside the boundary layer, which is about 1 cm deep at the end of the aerodynamic model table at a speed of 41.2 m/s) this condition unfortunately eliminates modelling of the natural wind gradient which is quite steep close to the surface of the sea – i.e. within the adjoining 3 m; thereafter, free stream velocity is essentially reached about 20 m up.[7] This aspect was one of several simplifications necessary in

the model testing – others (in hydrodynamic model testing) being the disregard of all natural ship rolling movements and various effects associated with the rudder, the propellor(s) and the driving machinery.

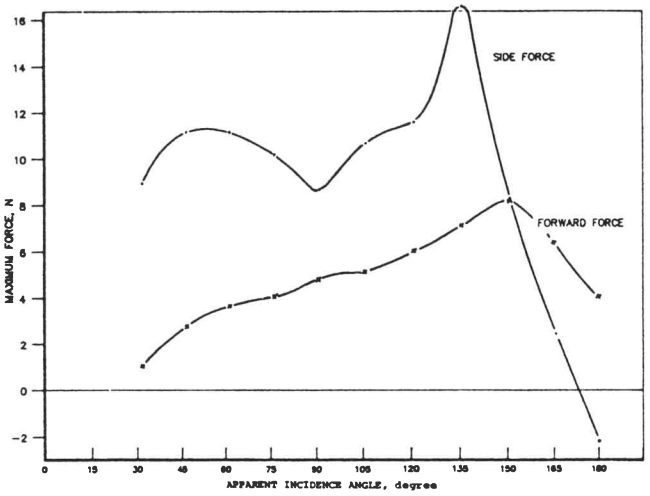

Figure 8 Aerodynamic tests – maximum force (at any sail angle) vs apparent incidence angle

Hydrodynamic testing

The towing tank employed was constructed from galvanised steel panels (Braithwaite plates), each 1.22 m square, giving a towing volume 15.86 m long, 2.44 m wide and approximately 1 m deep. External U-supports were provided for the tank at regular intervals, since tanks of this form are normally supported by internal cross-beams. The towing trolley (see Figure 9), supplied by Plint and Partners Ltd,[3] ran on two cylindrical rails, one above the other. Two pairs of wheels bore on the top rail and one on the lower; one wheel was driven by a variable speed low voltage D.C. motor through a reduction gear box, the maximum speed of the trolley being 1.2 m/s. Electrical connections to the trolley were made via a trailing cable, and speed measuring contacts 5.745 m apart also controlled a stop clock which had a resolution of 0.01 s. The trolley was brought to rest automatically at the end of its run (and the motor then reversed). The model support beam extended about 1 m over the tank and the two pins shown at the end of the model support in Figure 9 located in slots in the ship model. These pins enabled the model to float (vertical movement) and to pitch, but not to roll or list. To vary the ship model incidence γ, the adjusting screws in the model support column (Figure 9) were loosened to enable the ship to be rotated in order to be lined up with a mark at the end of the towing tank at a distance ($x \tan\gamma$) from the direction of towing (where x is the distance from the model at the position of adjustment to the end of the tank).A bi-directional load cell was attached to the support arm; this consisted of a steel beam of 5 mm square cross-section with strain gauges fitted to two adjacent faces to make up two orthogonal Wheatstone bridges to measure forces in two directions. The maximum load was 5 N, and output was plotted on a Watanabe Multicorder, using two pens. Calibration was effected by loading the tip of the model support with known weights in the forward and sideways directions. Because the transverse dimensions of the strain gauges were approximately equal to the 'load cell' width, a purely side or drag force affected both outputs [Figure 10(a) and (b)], and readings from both channels were required, for example, to determine drag force on the complete model for every test.

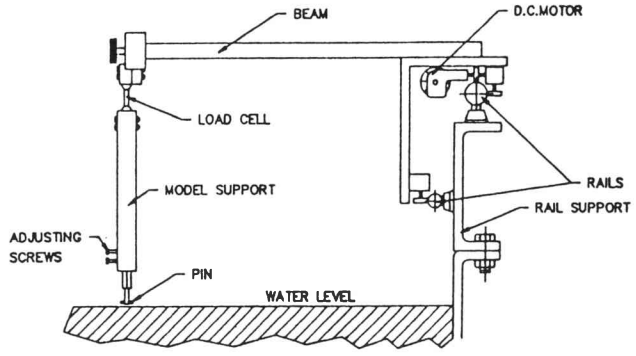

Figure 9 Schematic of towing trolley

Initial tests were conducted by towing the ship at zero angle of incidence at various speeds between 0.4 and 1.0 m/s. In each case the trolley was slowly accelerated up to the required speed on the Plint speed control, but care was taken to ensure that this speed was reached well before the trolley passed the first speed measuring contact – at which time the Multicorder pens were lowered to record the load cell output; the pens were raised again as the trolley passed the second contact. Thereafter the ship model was slowly returned to the starting point and the run time noted. Once the induced waves had died out sufficiently, the pens on the Multicorder were lowered to record a null value before commencing a further test. Further tests were then performed over the same speed range at various ship's angles of incidence.

A complete set of results for each run therefore consisted of:

1. Leeway angle of ship;
2. Run time, leading to model speed and hence Fr and Re; and
3. Multicorder outputs, leading to side force and drag measurements.

An average value of C_f was found using equation (6) (which assumed laminar flow over the wetted surface), from which a value of friction force was calculated – to be subtracted from the measured drag to yield residual resistance. Some typical results are presented in Figure 11 (drag versus speed for various leeway angles), Figure 12 (side force versus speed for various leeway angles), and Figure 13 (side force versus leeway angle for various speeds). The drag results ((particularly for 0° leeway angle) agree well with those given by the model manufacturer, as given

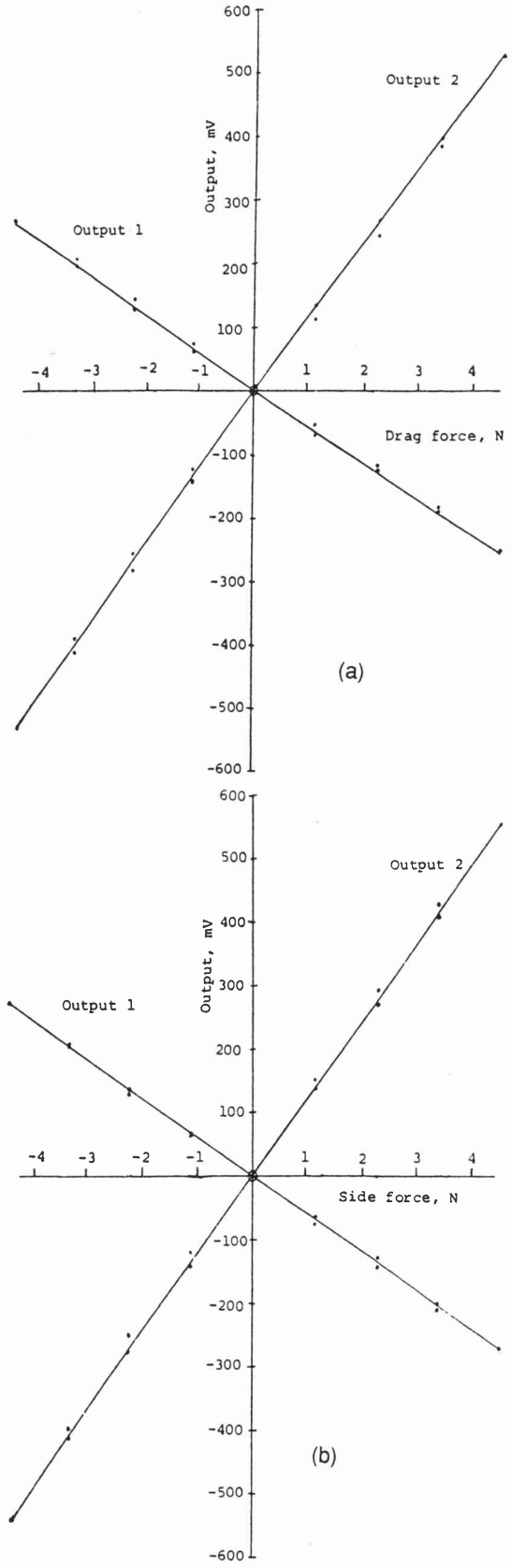

Figure 10 Hydrodynamic tests – calibration curves

in Appendix 3. The side force tests in particular illustrate the 'humps' and 'hollows' typical of wave-making resistance curves. (These are due to the fact that the wave pattern caused by a moving ship may be approximated in the first instance by a pressure source at the bow and a suction source at the stern. The transverse waves caused by these sources are superimposed, either increasing or decreasing the resisting effect of the wave pattern according to the speed and corresponding wavelength.) In the case of the side force measurements, the first hump occurs at a Fr number of $\frac{0.65}{\sqrt{9.785 \times 1.22}}$ or 0.188, and further humps may be expected at higher values of Fr.

Figure 11 has been plotted interms of force vs speed, whereas it is sometimes preferable to use a force coefficient, as used in Figure 6. Figure 11(d) compares C_T vs Fr for model results (both those obtained here and by the manufacturer) with full scale values.[3] Agreement can only be described as fair, however, while trends are felt to be more clearly brought out in the force vs speed diagrams of Figure 11(a) to (c).

Combined aerodynamic and hydrodynamic results

The results of forward force and side force obtained in the wind tunnel were for a stationary ship in an airflow of constant speed – equivalent to the effect of an **apparent** wind of constant speed acting on a ship in motion. Since the interest lay in the effect on a moving ship in standard conditions (i.e. constant **true** wind speed) at various angles of incidence, it was necessary to convert these results to apply for a constant true wind speed and therefore varying apparent wind speed as incidence angle varied. Such standard conditions were (see Model Design section and Appendix 1):

Prototype ship speed V_s	=	11.7 knots
(Average) prototype wind speed V_w	=	13.23 knots

From the following true and apparent wind velocity triangle,

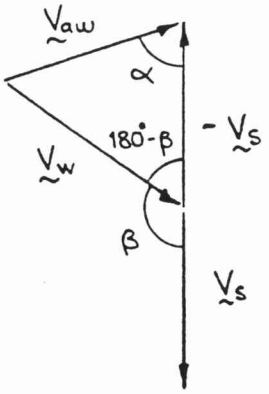

for each true incidence angle β, we have

$$V_{aw}^2 = (13.23)^2 + (11.7)^2 - 2(13.23)(11.7)\cos(180° - \beta) \tag{12}$$

and

$$\alpha = \sin^{-1}\left(13.23 \sin \frac{(180° - \beta)}{V_{aw}}\right) \tag{13}$$

Table 4 shows the results of this calculation for values of β at 15° intervals between 0° and 180°.

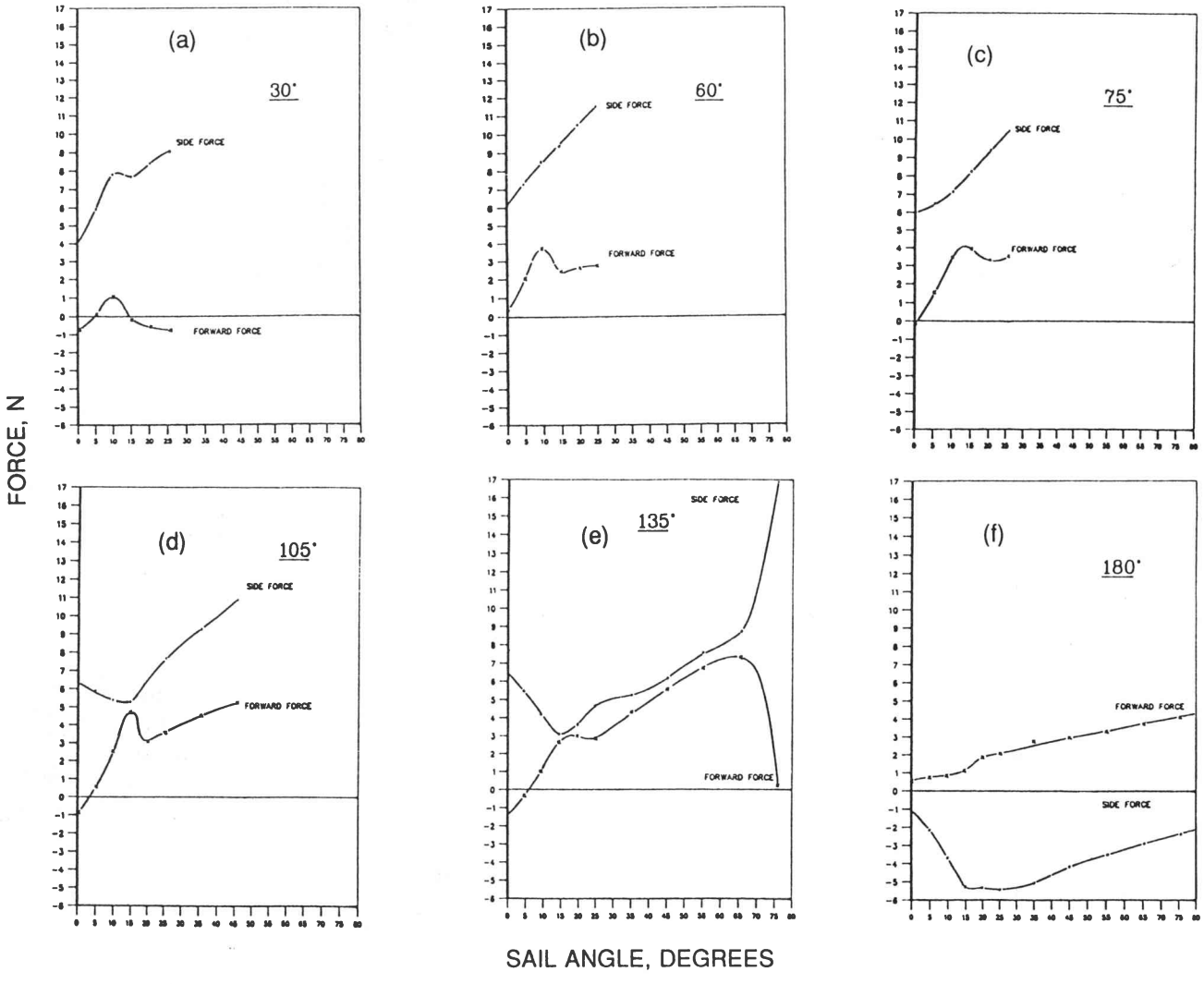

Figure 7 Aerodynamic tests – force vs sail angle for various incidence angles

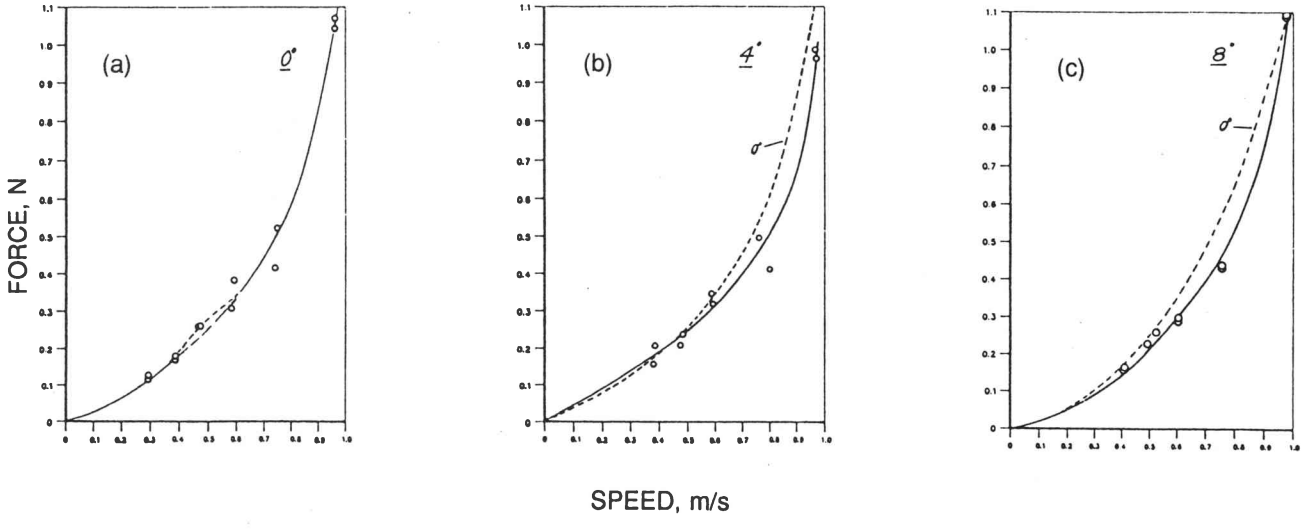

Figure 11 Hydrodynamic tests – drag vs speed for various leeway angles

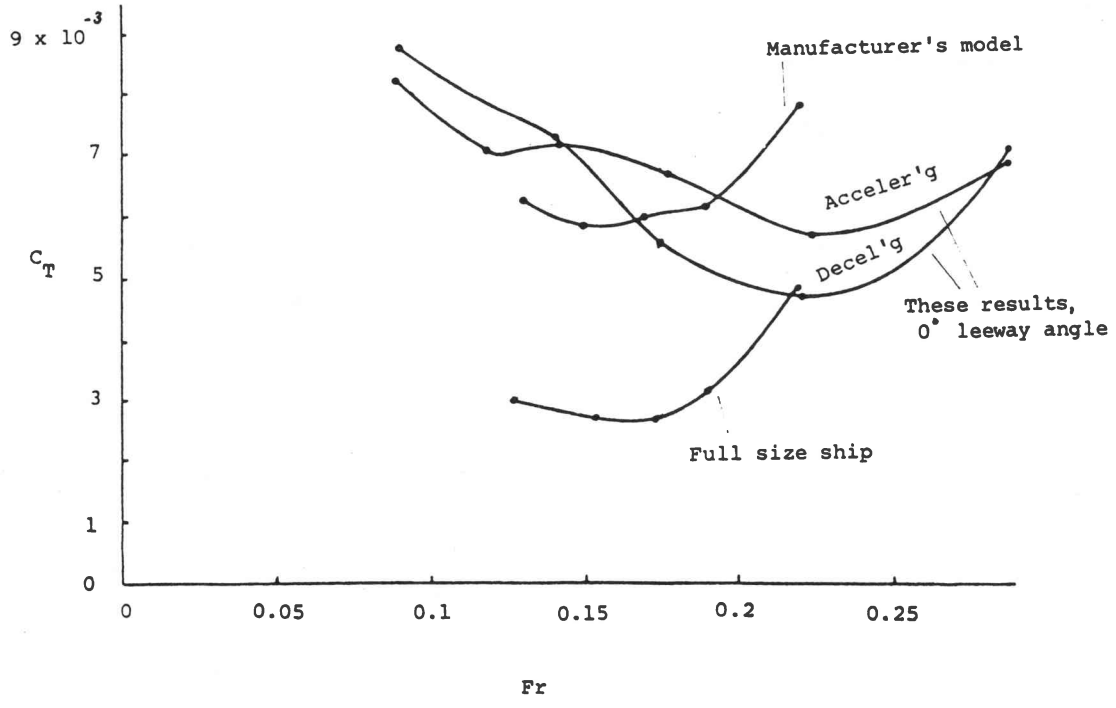

Figure 11 (d) Comparison of hydrodynamic results on $\frac{C_T}{Fr}$ basis

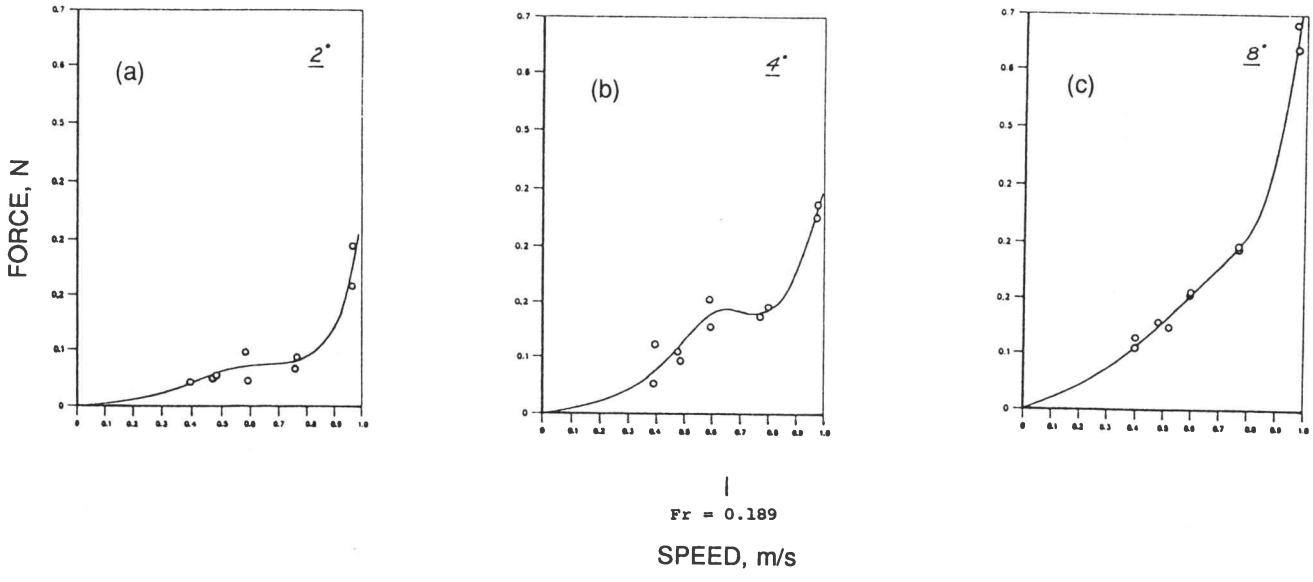

Figure 12 Hydrodynamic tests – side force vs speed for various leeway angles

Table 4 V_{aw}, β and the factor $\left(\frac{V_{aw}}{13.23}\right)^2$ for varying β

True incidence angle β, degree	Apparent wind speed V_{aw}, knot	Apparent wind angle α, degree	Factor $\left(\frac{V_{aw}}{13.23}\right)^2$
0	24.93	0.00	3.55
15	25.71	7.96	3.49
30	24.08	15.94	3.31
45	23.04	23.96	3.03
60	21.60	32.04	2.67
75	19.80	40.20	2.24
90	17.66	48.52	1.78
105	15.22	57.10	1.32
120	12.54	66.02	0.90
135	9.64	76.03	0.53
150	6.62	87.77	0.25
165	3.59	107.48	0.07
180	1.53	180.00	0.01

For each apparent incidence angle, the forward force at the optimum lift/drag ratio, together with the maximum forward force, was calculated, thus giving a curve of optimum forward force versus apparent incidence angle. This is given in Figure 14. Plotting the apparent incidence angle calculated above on the forward force curve, a maximum force was read off and scaled by the factor $\left(\frac{V_{aw}}{13.23}\right)^2$ to determine what this force would have been in the case of a constant true sind (since such force is proportional to the dynamic pressure $\frac{1}{2}\rho V^2$). These factors are also listed in Table 4. A graph of maximum forward force against true incidence for a ship moving at $\frac{11.7}{13.23}$ of the true wind speed can thus be obtained (Figure 15).

For incorporation with the aerodynamic results, the hydrodynamic results were first scaled up to full size, as follow:

- Total resistance of the model at a towing speed of 0.6 m/s was obtained at 0° leeway angle.
- The calculated friction force was subtracted from this to give the residual force.
- The residual force was scaled up, using the ratio of displacements.
- The full scale friction force was calculated and added to the scaled up residual force to give the total resistance of the ship – which might then be compared with the maximum sail lift. (The aerodynamic resistance of the hull was neglected since in terms of dynamic pressure, it was only about 3.3% of the hydrodynamic resistance at 11.7 knots.)

An example of this calculation follows:
For the model towed at 0.60 m/s (the equivalent of a full scale ship travelling at 11.7 knots at the same value of Fr) and 0° leeway angle [Figure 11(a)] in sea water,

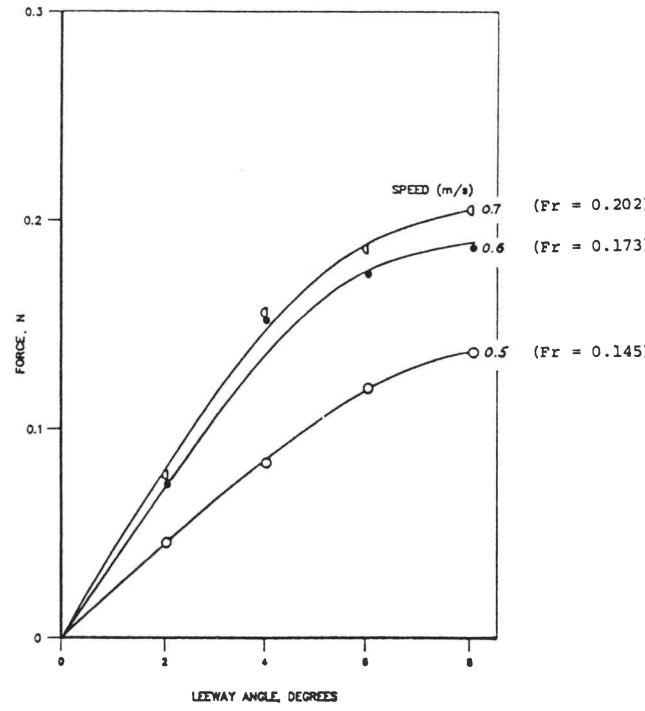

Figure 13 Hydrodynamic tests – side force vs leeway angle for various speeds

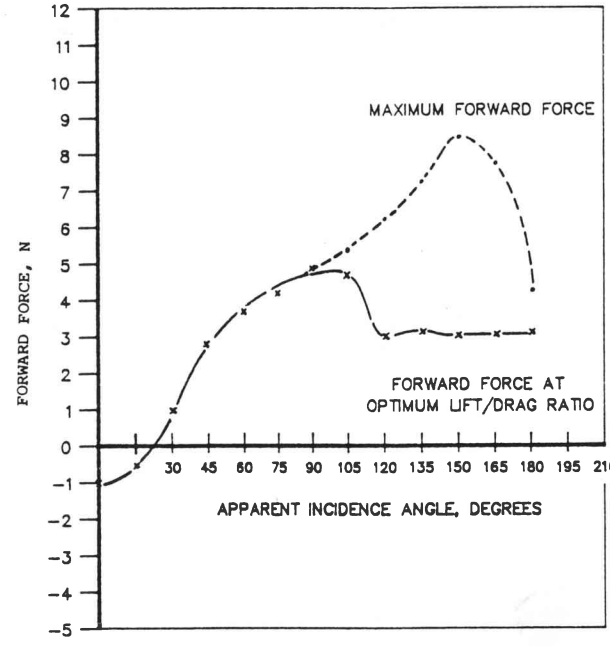

Figure 14 Forward force vs apparent incidence angle α at optimum sail angle (apparent wind speed constant, with ship stationary)

Residual resistance	=	0.137 5 N
For full-sized ship, residual resistance	=	$(100)^3 \times 0.137\,5$
	=	137 000 N
Reynolds number at 11.7 knots (sea water)	=	6.67×10^8
whence C_f from eq.(6)	=	1.61×10^{-3}

Therefore

$$\begin{aligned}\text{Skin friction} &= \tfrac{1}{2}\rho V^2 A C_f \\ &= (1\,025)(6.02)^2 \times 1.61 \times 10^{-3}\,[0.254 \times 100^2] \\ &= 76\,040 \text{ N} \\ \text{Total resistance} &= 137\,000 + 76\,040 \\ &= 215\,540 \text{ N}\end{aligned}$$

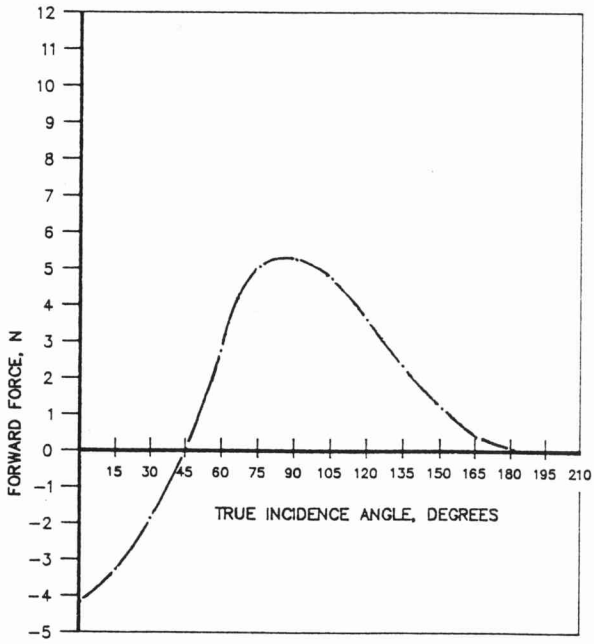

Figure 15 Forward force vs true incidence angle β at optimum sail angle (true wind constant, with ship moving at 88% of wind speed)

Testing of complete hydrodynamic model in 'fan wind'

In an attempt to justify the deductions made so far, a further test of a towed model of 1:300 scale, with sails, was made in a towing basin, using a fan mounted on a bracket attached to a 4-wheel towing trolley to provide a simulated wind. Model force was similarly measured by means of strain gauges on the support beam. The fan could be swivelled about the model ship to give apparent incidences α from 45° to 180°. The model speed was kept constant at 0.32 m/s (corresponding to a full scale value of 10.64 knots), the average wind speed – the only speed available with the motor used – being 6.55 m/s (or 12.58 knots) on the flow axis. (This model was free to heel.)

The results for forward force and side force as a function of apparent incidence α are given in Figure 16. (Only maximum values are shown, as before, regardless of sail angle.) These results are qualitative only, in the sense that no real consideration could be given to scaling wind speed in relation to model speed. Nevertheless, the curves of Figure 16 are generally similar to those of Figure 8. Actual peak force values are somewhat lower for forward force, and considerably lower for side force. The maximum forward force occurs at a condition with the wind fully astern ($\alpha = 180°$), rather than at $\alpha = 15°$, which suggests that the sails are then operating in a drag, rather than a lift, mode, i.e. fully stalled.

Prediction of fuel savings

Proportional fuel savings were estimated from the following expression:

$$\text{Savings} = \frac{\text{scaled up max. aerod. forw. force (sails) at true wind incid. value}}{\text{Thrust to propel full size ship (total resistance)}} \qquad (14)$$

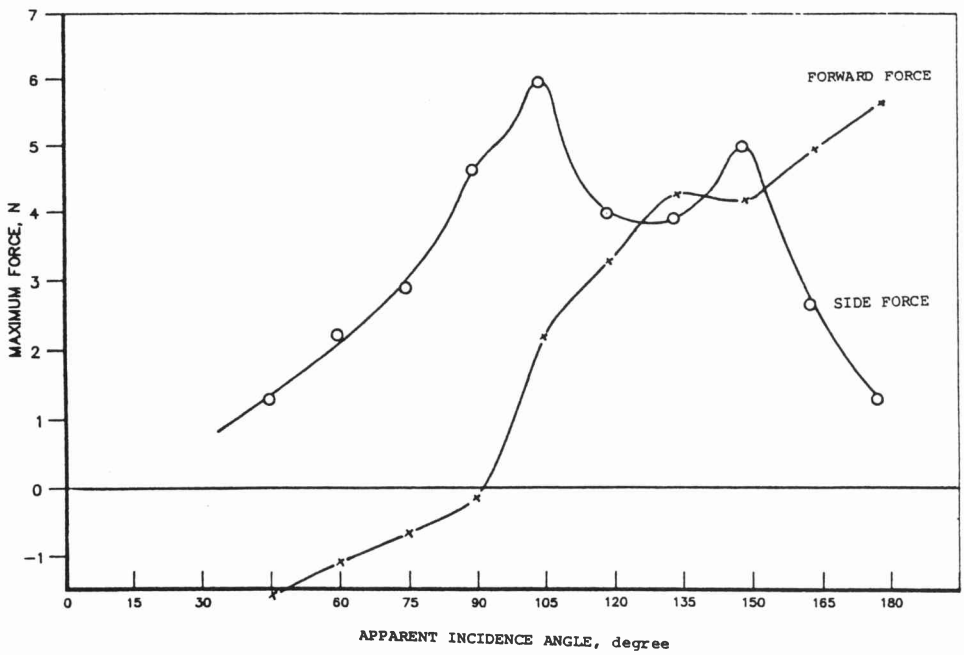

Figure 16 Forward and side force vs apparent incidence angle α (with simulated wind)

Example of calculation

For wind tunnel model at 90° true incidence and 31.93 m/s speed – at which the dynamic pressure is 0.6 kPa – then from Figure 15,

Maximum forward force = 5.198 N

Since this force = (dynamic pressure) (model area),

Model area = $\frac{5.198}{0.6\times10^3}$ m^2

Therefore

Prototype forward force at 13.23 knots

$$= \tfrac{1}{2}\rho V_w^2 \text{ [model area]}$$
$$= \frac{0.5(1.177[6.81]^2\ 300^2\times5.198)}{0.6\times10^3}$$
$$= 21\,280 \text{ N}$$

Therefore

Savings = $\frac{21\,280}{213\,500}$ or 9.97%

By calculating this proportion for each true incidence angle from 0° to 180°, the polar diagram shown in Figure 17 was obtained.

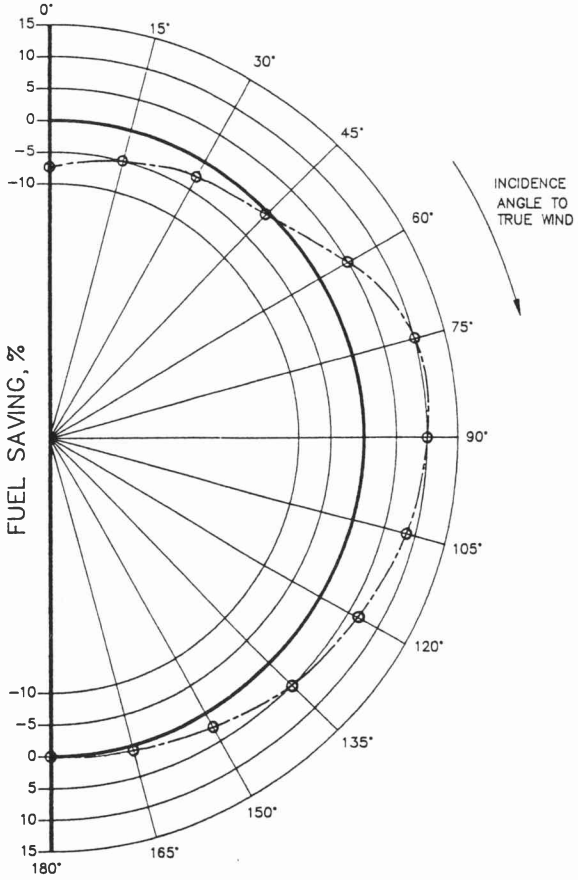

Figure 17 Calculated fuel savings at various incidences from 0° to 180° for 'standard' conditions

Discussion

Aerodynamic results

Forward and side force versus incidence angle for ship without sails (Figure 6)

In general, the side force curves show an expected large increase up to 90° incidence angle, followed by a decrease to approximately zero at 180°. The peak at 180° was unexpected; this may be connected with the particular shape of the superstructure. More probably, however, since the yawing moment (not recorded here) also increases in this region and peaks at 120°, it may be concluded that there was an interaction between the measurements. In the case of the smaller forward force measurements, a similar explanation is believed to account for the trough at 120°.

Forward and side force versus incidence angle for ship with sails (Figures 7 and 8)

At values of incidence less than 30°, forward force values were all negative (and are not therefore illustrated, since the use of sails is then disadvantageous). Figure 7(a) shows that a positive forward force is possible at an incidence value of 30° (and Figure 14 indicates that advantage may be gained from the use of sails at as low an angle as 25°). In Figure 7(a) it appears that the stalling angle has dropped from 16° for the ideal 2-dimensional aerofoil (Figure A-1) to about 10° – an example of 'scale effect' – but may also be due to interference between the sails (see Figure 18). Specifically, the disturbed air and vortices leaving the trailing edge of aerofoil 1 have the effect of promoting separation on the leeward side of aerofoil 2, thus causing stall to occur sooner than anticipated. This effect is encouraged as the sail angles increase as this brings the aerofoils closer together and the 'slot' between them closes (Figure 19). Had this effect been more fully appreciated at the time of testing, it would have been interesting to have conducted tests with only one aerofoil in operation and thus to compare results to determine whether the effect of two aerofoils is more than twice that of one aerofoil – i.e. to determine whether the interference and associated lowering of the stall point has a positive or negative effect.

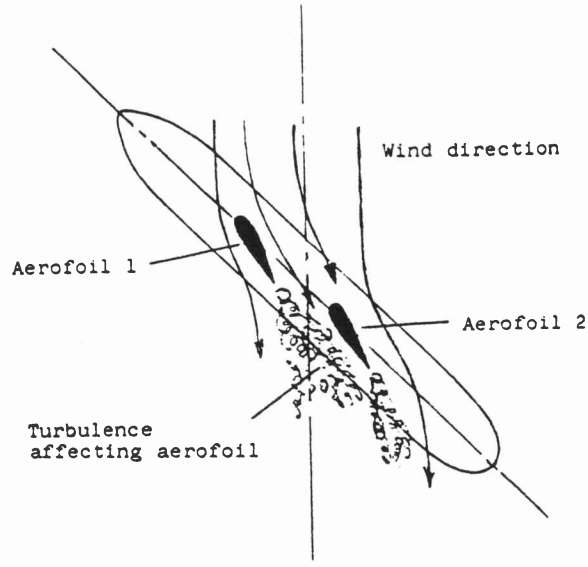

Figure 18 Interaction between sails

Examination of the side force plot on Figure 7 (a) shows a peak corresponding to the stall point, together

with a point on inflection, after which side force increases steadily. This peak in side force is small compared with the peak in forward force at this point, so it would seem that this must be the optimum operating point for this incidence angle. As the incidence angle increases up to 60° [Figure 7 (b)], so the forward force increases correspondingly, although the stall point remains in the region of 10°. The aerofoils are thus giving rise to a large amount of interference, but unfortunately it is impossible to determine the exact angle of the stall with so few results. The peak in side force at the stall point has now virtually disappeared and the increase in side force is almost linear with increase in sail angle (and constant with increase in incidence angle).

Considering now the effects shown in Figure 7 (c) and (d), it is noted that the stall point increases and eventually attains the theoretical value of 16°. The abruptness of the stall has now definitely increased and the peak forward force value almost reaches 5 N. This clearly indicates that, since the angles of the aerofoils relative to the ship have now dramatically increased, the aerofoil clearance is greater and the aerofoils are thus less susceptible to interference from each other (see Figure 19). The aerofoils may now be acting more independently and so be following the characteristics of Figure A-1 more closely. However, the forward force is still low in relation to the theoretical ideal lift under these conditions (which can be shown to be 9.6 N). The main reason for this would appear to be the low sail aspect ratio employed.

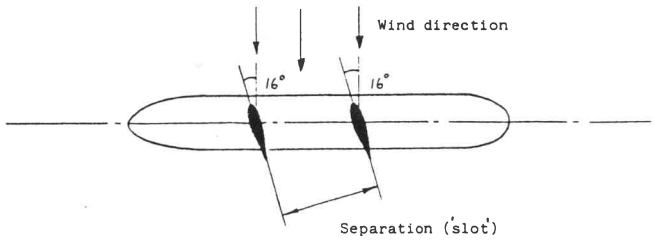

Figure 19 Increased separation of the sails

At 105°, the side force curve began to show a deep trough corresponding to the stall point. This probably indicates a higher efficiency of aerofoils now able to act independently, and thus the greater ease with which the ship may be sailed at such incidence angles. As the incidence increases up to 150° [see Figure 7 (e)], the stall point at about 16° becomes less and less significant. The forward force increases steadily with sail angle and a new, much larger, value of pseudo-stall angle becomes evident at a sail angle of about 65°. Since this is well beyond the stall point of the aerofoils, the condition for maximum forward force is now manifested in high drag values for the aerofoils rather than in high lift values. Above an incidence value of 150°, the forward force actually begins to decrease, due to aerofoil 1 moving into the 'wind shadow' of aerofoil 2 [see Figure 7 (f)]. This would indicate that an advantage can certainly be gained by pointing the sails to opposite sides of the ship, as shown in Figure 20. To demonstrate this point, further tests were made, as shown in Table 5; these show that a 25% increase in forward force (as given by 5.054 7 N, as compared with 4.057 6 N) is thereby made possible.

Since it is clear from this case that performance can be improved by setting the sails at unequal angles, improvement should be possible at other incidence angles – particularly as one aerofoil often experiences a different apparent wind angle due to the disturbance caused by the other; the optimum setting of one may thus well not be the optimum setting of the other. Many more tests are thus required to establish a true optimum forward force curve – since Figure 14 only indicates the optimum for equal sail angles.

Another factor which disturbed the reading at high incidence angles was a distinct buffeting experienced by the sails. At high incidence angles, when the sails were set close to 90° sail angle, the division of the oncoming air flow by the sail 'obstruction' created a large amount of turbulence (see Figure 20) – to avoid which a stiffer sail pivot is required than was provided.

Table 5 Effect of reversal of sails for ship incidence angles of 180°

Sail angle, degree		Forward force, N	Side force, N
1	2		
Sails aligned			
75	75	4.033 1	−0.109 5
85	85	4.235 4	−0.848 2
95	95	4.111 1	−1.630 2
90	90	4.180 5	−1.034 7
105	105	4.057 6	−2.429 1
Sails reversed			
255	85	4.180 5	−1.034 7
265	85	5.368 3	0.121 4
270	85	5.246 9	−0.347 7
280	85	4.816 3	−0.376 6
275	90	5.054 7	−0.369 3

Hydrodynamic results

Calibration effects

The towing tank force transducer was calibrated by attaching a line to the model support pin and loading it in the required direction using known masses. As stated earlier, because the transverse dimension of the strain gauges were approximately equal to the load cell width, a purely side or drag force affected both outputs, as shown in Figure 10. (Readings from both channels were therefore required to determine the drag force for every test.) During calibration, forces up to 5 N were applied in opposite directions. At specific loadings, the reading differed by as much as 5% on either side of the means. This hysteresis effect could have been due to plastic deformation of the wax used to

cover the strain gauges, and, together with changes in the bridge excitation voltage, this varied the null outputs by as much as 30 mV during calibration. A null reading was therefore taken before each; this also allowed the water surface conditions to be estimated quantitatively. Since the model's longitudinal section was much larger than its transverse section, Output 2 was the most affected by surface disturbances.

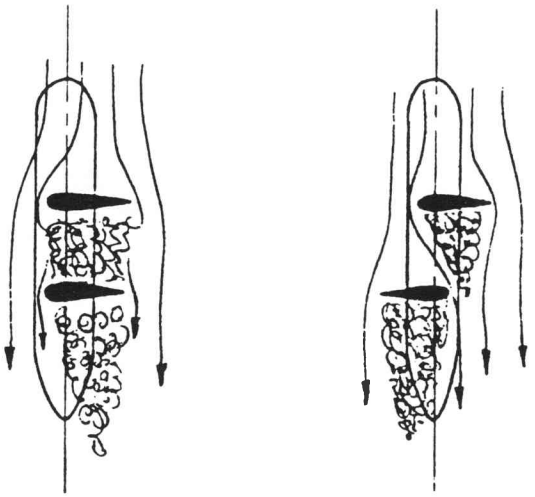

Figure 20 Advantage from reversed sail angles

The voltage outputs during runs were characterised by a noise signal superimposed on sinusoidal mean lines. The noise signal was similar for all tests – indicating that it was a characteristic of the basic equipment used and so would have been difficult to eradicate. However, the variation of the mean line appeared to be due to induffi-cient alignment of the carriage rails (first raising and then lowering the model during a run). This made the determination of the average output difficult, and introduced positioning errors of ±2 mm. If the rails had been further straightened, the reading error might have been halved in spite of the noise. The use of an integrating voltmeter on both channels would also have helped to standardise the data acquisition procedure and so yield more consistent results. Finally, it appeared that the tank should have been allowed to settle for at least 15 min between runs to ensure satisfactorily smooth conditions.

Drag versus speed results (Figure 8)

The fact that drag increased extremely rapidly with speed is illustrated in Figure 8 (a) for the case of a 0° leeway angle. For example, the force doubled when the towing speed was increased from 0.835 to 0.990 m/s. Comparison of the average and measured drag curves reveals initial evidence of the existence of the distinctive 'humps' and 'hollows' in the total resistance curves caused by wave resistance. For the speed range investigated ($0.1 < Fr < 0.3$) these effects are relatively minor, but nevertheless change residual resistance by up to 20%. The chosen standard speed of 11.7 knots (0.6 m/s model speed) is evidently associated with a hump, and 15 knots (0.78 m/s model speed) would seem to have been a more desirable speed from this point of view. The readings between 0.5 and 0.9 m/s seem to be the least reliable, as shown by the scatter; this may have been caused by difering boundary layer flows (laminar or turbulent) in each test, as the corresponding Reynolds numbers are near the transition value of 10^6.[8] The nature of the boundary layer is critical in tests on small models as the ratio of friction to residual resistance is large.

Compared with the standard RINA YB Tanker results,[3] the total drag figures estimated are approximately 20% too high. This is ascribed to

1. possible yawing of the model;
2. small misalignment of the rails, causing the model to rise and fall in a periodic manner; and
3. the presence of scum floating on the water surface.

Because of the small residual resistance experienced by the model, this over-reading could predict a total ship resistance approximately 100% too large at 11.7 knots.

When the drag at leeway angles between 2° and 8° is compared with the mean drag [Figure 8 (b) and (c)] no coherent pattern emerges. Contrary to intuition, towing the ship at a leeway angle of 2° (not illustrated) actually reduced the indicated total resistance by up to 40% at 0.4 m/s. At 4°and 6° leeway angles, the results are similar to the 0° case, while at 8° leeway, the resistance is again lowered by up to 20% at speeds around 0.7 m/s. Since individual readings at each angle were compatible, and care was taken to maintain a consistent testing procedure, these curious results are probably due to a major change in the nature of the boundary layer flow. On the 'windward' side, the pressure gradients would maintain laminar flow, while on the 'leeward' side, turbulence could have been highly developed; this could have effectively lowered the average value of skin friction, as suggested in Figure 21.

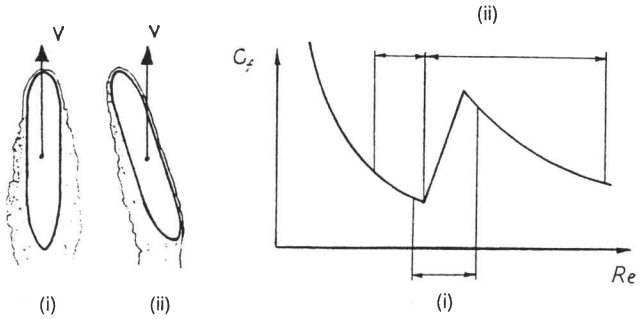

Figure 21 Possible boundary layer effects

A further factor is that the centre of hydrodynamic force did not coincide with the model support. This created a twisting moment on the narrow load cell, which allowed a change in leeway angle of up to 1° to occur during a run; this moment could have affected the load cell output

if the strain gauges were not mounted perfectly perpendicular to the vertical axis. This effect was most pronounced at the higher leeway angles, when forces were greatest. Finally, the angled model created considerable sidewash at high speeds. Interaction with the walls (spaced 1.2 m apart) would increase the measured side force, while reducing the indicated drag, due to the inter-dependence of the load cell outputs. Again, this effect would have been greatest at high speeds.

No strong conclusion may therefore be drawn concerning the effect of leeway angle on drag. However, it was expected that the additional resistance associated with 'drifting' sideways would approach the drag of a low aspect ratio hydrofoil.

Side force versus speed results (Figure 12)

The relationship between side force and speed for various leeway angles is shown in Figure 12 (a) to (c). The curves appear to be similar to the normal ship drag curve with humps and hollows at corresponding speeds. Because the magnitude of the humps varies and of the fact that they alternate with increased leeway angle, it seems that drag has little influence on the indicated side force. Instead, it is probable that the pressure field associated with a particular wave system influences the boundary layer behaviour, and so ultimately the side force. Consider the case of a 4° leeway angle [Figure 12 (b)]; up to 0.6 m/s the curve is similar to the 8° line, while thereafter it approaches the 2° line. This could indicate the occurrence of a transition from a flow along the sides (generating side force) to a flow along the bottom, giving less lift; such a case is analogous to the stall of an aerofoil. Assuming that such flow is related to the value of the Reynolds number means that the results cannot be accurately scaled since full scale and model Reynolds numbers differ by a factor of 10^3 – which is especially important with a model operating in the transition region. Fortunately, the effect of wave drag is reduced at greater leeway angles, and the force curve tends to an increasingly parabolic shape. This seems to justify the assumption that the hull acts as a low aspect ratio hydrofoil. This is illustrated in Figure 13, where the side force is plotted against leeway angles. The force is proportional to incidence for small angles, but the curve flattens as lift, and therefore tip circulation, increases – which is similar to the behaviour of the square-rigged sails of the 19th century.

Combination of aerodynamic and hydrodynamic results

The results presented were calculated using the following simplifications to enable conclusions to be reached with the facilities available:

1. Standard wind speed of 13.23 knots
2. Standard ship speed of 11.7 knots
3. Zero leeway angle
4. No drag increase due to side force

The selection of standard conditions does not restrict the usefulness of the results, as a new polar fuel savings diagram similar to that of Figure 17 can be rapidly produced for any wind and ship speed, using the forward force versus apparent incidence angle type of graph shown in Figure 14. For a non-zero leeway angle, the apparent wind angle would be reduced by this amount. The curve of forward force vs true incidence angle (Figure 15) will therefore be shifted over, depending on the magnitude of the drift. A 'correct' solution would have to be obtained iteratively, using accurate data on the relationship between side force, speed, and leeway angle. Finally, the leeway angle would usually prove to be so small (say $< 5°$) that the change would be less than the error inherent in the experimental method.

The most serious weakness of this investigation was its inability to quantify the drag increase due to side force. According to the wind tunnel tests, the side force is greater than the forward force at 30° apparent incidence by a factor of 8, while they are of similar magnitude only after 135° apparent incidence. This situation is exaggerated by the effect of ship speed in moving the apparent wind forward of the true wind. The drag resulting from the sideways force would therefore be considerable even for a highly efficient hydrofoil, and should be added to the total hydrodynamic resistance before calculating effective drag reduction. Finally, a non-zero leeway angle would result in the propellor force being misaligned to the direction of travel, while rudder corrections would increase drag. The fuel savings would therefore be less than predicted in Figure 17.

However, careful route planning (an astute combination of ship speed and direction) should enable the maximum calculated fuel savings of 10% to be exceeded on a typical journey. For instance, in medium wind conditions a ship would sail in a direction approximately perpendicular to the true wind to raise the apparent wind speed, while limiting side force; this is shown in Figure 15. As the true wind speed increases, the ship speed will affect the apparent wind speed less, and the forward force vs true incidence curve will tend towards that of Figure 14, i.e. the optimum true incidence will be as much as 150°. Conversely, a high ship speed will have the effect of bringing the optimum incidence forward, and so raising the side force dramatically. This would seem to discourage the use of sails for large, and thus fast, vessels.

Conclusions and recommendations

Aerodynamic (sails) and hydrodynamic (hull) test results were combined to calculate approximate percentage fuel savings for wind incidence angles from 0° to 180°. Under the chosen conditions (over a North Atlantic route, using a wind of average strength and direction), it was found that a maximum fuel saving of about 10% was possible for a wind on the beam and sail angles of 10°. Only a narrow

range of the latter was found to be sufficiently effective to justify use, thus indicating that careful and continuous sail control (as a function of wind direction) would be required. In general, the ideal route should have a mean wind direction 90° to 110° off the ship's course, while regular strong winds could have true incidences as high as 150°. (To choose a route, a family of net forward force vs true incidence curves, as shown in Figure 15, should be drawn, each line representing a particular wind speed. Surface wind conditions obtained from routing charts or directly from weather models could then be utilised to determine the average forward force over a chosen route.)

The savings results predicted by this experiment fall far short of the claim [2] that the Japanese vessel's sails can provide up to 50% of the power required to travel at 12 knots. However, the wind conditions on which this figure was based might have been very different: south of Japan, the prevailing wind direction is N or S, and the ship may have been travelling in a 'drag mode' (with a wind incidence of up to 180°) to achieve such a result.

In addition to the conditions investigated, various other possibilities could usefully be examined in further tests, for example:

- The use of different sail configurations, such as the use of a single aerofoil (to evaluate interference); the use of sail end plates to improve 2-dimensionality; the use of aerofoil slats, flaps and other variable geometry devices; and testing under conditions where the sails are each set at their respective optimum angles.
- Changes in the hydrodynamic model configuration, such as the use of turbulent wire 'trips', a larger model, and a more rigid form of attachment to prevent pitching.

References

[1] Anon. Catamarans with aerofoil sails. *New Scientist*, 17 November 1990.

[2] Anon. *Special Report, Energy.* National Geographic Society, Washington, DC, 1981, p.38.

[3] Towing tank instruction manual TE 89/A, Plint & Partners Ltd, Wokingham, England, 1985.

[4] Abbot IH & von Doenhoff AE. *Theory of Wing Sections.* Dover Publications, New York, NY, 1959.

[5] Comstock JP (ed.). *Principles of Naval Architecture*, Revised edn, Society of Naval Architects and Marine Engineers, New York, NY, 1967, p.298.

[6] Goldstein S (ed.). *Modern Developments in Fluid Dynamics*, Vol. II. Oxford University Press, 1952, p. 365.

[7] Comstock JP. *Ibid.*, p.317.

[8] Blevins RD. *Applied Fluid Dynamics Handbook.* Van Nostrand-Reinhold Co., New York NY, 1985, p.317.

[9] Moor DI. The © of some 0.80 C_b forms. *RINA Transactions*, 1960, **102**, 93.

Appendix 1. Choice of aerofoil type and size

The reasons for the choice of aerofoils section used here have been given under Model Design. Using the average prototype wind speed value $V_{aw} = 13.23$ knots and direction 117°, then from [3], at 6 m/s (11.7 knots), $R_t = 156$ kN.

From Figure 2 (a),

$$\begin{aligned} V_{aw} &= \left[\begin{array}{l} (11.7)^2 + (13.23)^2 - 2 \times 11.7 \\ \quad \times 13.23 \cos(180° - 117°) \end{array} \right] \\ &= 13.1 \text{ knots} \\ &= 6.7 \text{ m/s} \end{aligned}$$

Also

$$(13.23)^2 = (11.7)^2 + (13.1)^2 - 2 \times 11.7 \times 13.23 \cos\alpha$$

Therefore

$$\alpha = 64.5°$$

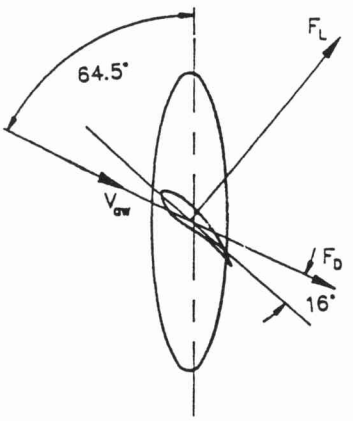

These values are taken as standard conditions for calculation purposes. From wing section data (Figure A-1), at angle of attack = 16°, $C_L = 1.5$ (max) and $C_D = 0.02$ (projected),

$$\begin{aligned} F_L &= \tfrac{1}{2}\rho V_{aw}^2 A\, C_L \\ &= 0.5\,(1.177)\,(6.7)^2\,(1.5)\; A \\ &= 39.6\; A\; N \end{aligned}$$

$$\begin{aligned} F_D &= \tfrac{1}{2}\rho V_{aw}^2 A\, C_D \\ &= 0.5\,(1.177)\,(6.7)^2\,(0.02)\; A \\ &= 0.528\; A\; N \end{aligned}$$

Therefore

$$\begin{aligned} \text{Forward force} &= FL\cos(90° - 64.5°) - FD\cos 64.5° \\ &= 35.51\; A\; N \end{aligned}$$

Therefore

Sail area for 20% reduction in R_t is given by

$$A = \frac{0.2 \times 156 \times 10^3}{35.51} = 878 \text{ m}^2$$

For the aerodynamic model at a scale of 1:300,

$$\text{Model sail area} = \frac{878}{(300)^2} = 0.009\,8\ \text{m}^2$$

which corresponds closely to the model sail area (elevation) of 2 × 50 mm ×100 mm. Details of milling co-ordinates are shown in Table A-1.

Table A-1 Milling co-ordinates for construction of aerofoils

x (mm)	*y* (mm)	*x* (mm)	*y* (mm)
0	0.00	42	15.52
11	11.10	43	15.55
12	11.15	44	15.57
13	11.25	45	15.55
14	11.37	46	15.52
15	11.50	47	15.49
16	11.65	48	15.48
17	11.82	49	15.42
18	12.00	50	15.25
19	12.19	51	15.13
20	12.39	52	15.00
21	12.59	53	14.86
22	12.80	54	14.72
23	13.01	55	14.57
24	13.23	56	14.40
25	13.44	57	14.21
26	13.55	58	14.00
27	13.75	59	13.76
28	13.94	60	13.48
29	14.21	61	13.16
30	14.29	62	12.80
31	14.45	63	12.38
32	14.60	64	11.88
33	14.74	65	11.30
34	14.88	66	10.64
35	15.01	67	9.90
36	15.13	68	9.08
37	15.23	69	8.12
38	15.32	70	6.70
39	15.40	71	4.70
40	15.46	72	0.00
41	15.49		

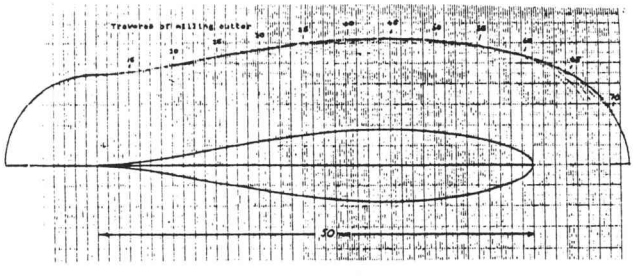

Appendix 2. Some details of YB Tankers

Although described by the model manufacturers as an 'RINA Standard Tanker, model YB', the reference [9] to the design refers to the YB form as being derived from the BSRA 0.74 C_b (= block coefficient), tested at the Towing Tank of the Ship Division of the National Physical Laboratory, St Albans, England. Figure 3 shows a plan and elevation of the model tested, and Figure 4 a photograph of the (waterline) test model with aerofoils fitted.

A 'body plan' for three forms (including YB) from [9] is given in Figure A-2.

Appendix 3

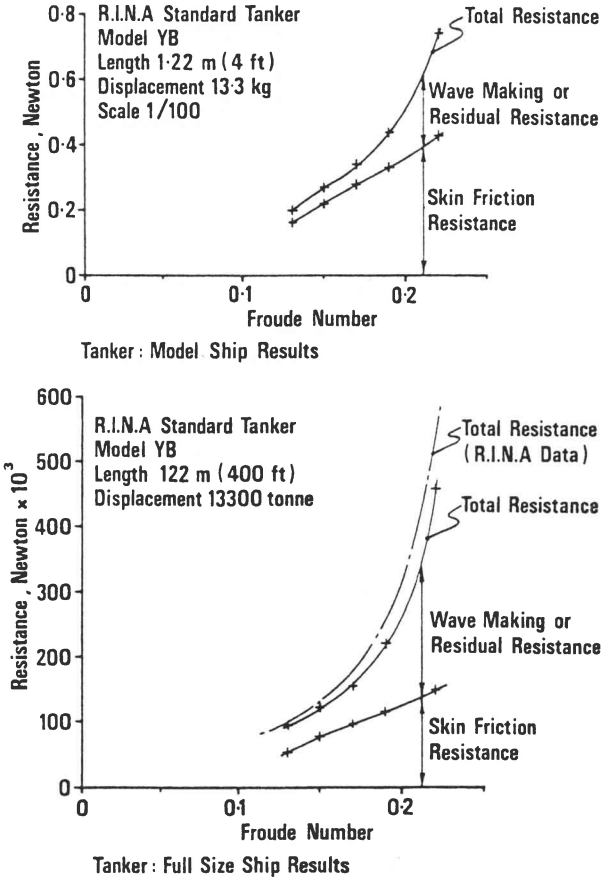

Figure A-3 Model and full scale tanker results [3]

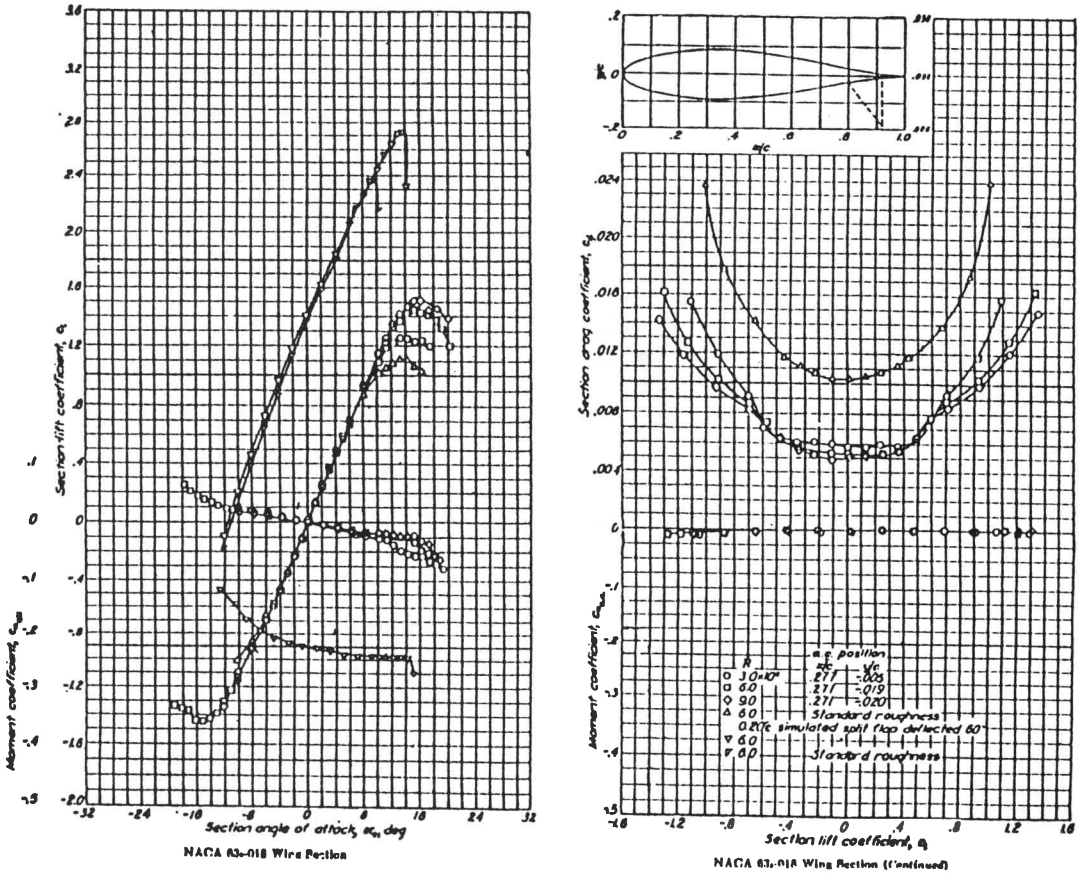

Figure A-1 NACA $63_3 - 018$ (2-dimensional) wing section characteristic [4]

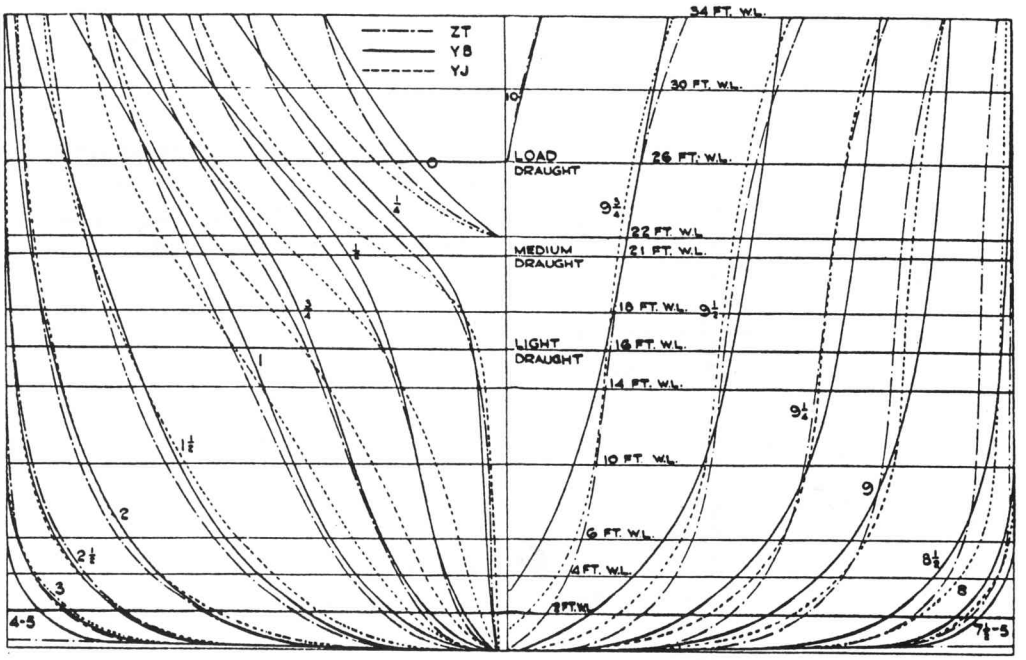

Figure A-2 'Body plan' for Models ZT, YB, and YJ [9]